

Investigation of AZ91D Magnesium Alloy Corrosion Behavior under Thin Electrolyte Layer Using Nondestructive Electrochemical Techniques

Linlin Nie¹, Yan Xia¹, Yaru Zhou¹, Junxi Zhang², Fahe Cao^{1,*}, Jianqing Zhang¹

¹ Department of Chemistry, Zhejiang University, Hangzhou 310027, P. R. China

² Shanghai Key Laboratory of Materials Protection and Advanced Materials in Electric Power, Shanghai University of Electric Power, Shanghai 200090, P. R. China

*E-mail: nelson_cao@zju.edu.cn

Received: 30 October 2015 / Accepted: 20 November 2015 / Published: 1 December 2015

In order to investigate the corrosion behavior of AZ91D magnesium alloy under thin electrolyte layers (TELS) in 3.5 wt. % NaCl solution during short immersion time, some nondestructive electrochemical measurements such as the electrochemical impedance spectroscopy (EIS), electrochemical noise (EN) and cathodic polarization curves were conducted. In addition, scanning electron microscopy (SEM) attached with energy dispersive X-Ray spectroscopy (EDS) and Scanning Kelvin Probe Force Microscopy (SKPFM) were employed to character the microstructure and the Volta potential distribution of AZ91D magnesium alloy surface. The experimental results reveal that the corrosion rate of AZ91D under TELS is slower than that in bulk solution and decreases with the TEL thickness thinning. Both the anodic and cathodic reactions were restrained under TELS, especially in thickness thinning to around 200 μm and lower. Furthermore, pitting corrosion is initiated at the matrix adjacent to the noble β phase particles and crevice corrosion is dominant at the early corrosion stage under TEL.

Keywords: Atmospheric corrosion; TEL; AZ91D alloy; Electrochemical technique; Corrosion behavior

1. INTRODUCTION

As well known, the nature of atmospheric corrosion is electrochemical processes between micro-galvanic couples under TELS. The corrosion behavior is closely related to the electrolyte layer thickness with the effects on transformation of dissolved oxygen, dissolution of metal which correspond to the cathodic and anodic process of metal corrosion respectively [1,2]. However, due to the huge ohmic drop between the working and reference electrodes and the uneven current distribution

on the working electrode, the atmospheric corrosion rate is difficult to determine accurately by electrochemical method, which limited the further study. Fortunately, Nishikata and coworkers [3] have proposed that if the phase angle exceeds -45° in Bode plot of EIS, the current distribution is uniform on the electrode surface. The TELs equipment used by our group [4] can minish the ohmic drop to a great extent and measure the TEL thickness with the accuracy of 10 μm .

Compared to other commercial metal materials, magnesium and its alloys have attracted more attention due to the outstanding properties such as low density, high specific intensity, excellent heat exchange, biocompatibility and electromagnetic shielding performance. In spite of the excellent properties, magnesium alloys show poor corrosion resistance in atmospheric environment, which results in huge losses and restricts their further application. In recent years, many works have been done on the corrosion behavior of Mg and its alloy in bulk solution [5-8]. However, the corrosion behavior study of magnesium alloy in atmospheric environment is not sufficient.

The corrosion behavior research of AZ91D, as one of the most widely used magnesium alloy, attracted a wide spread attention. Song et al. [9] studied the corrosion behavior of three different magnesium alloys in sodium chloride and proposed that the microstructure showed an effect on the corrosion behavior with the β -phase acting as an effective cathode to accelerate the corrosion of matrix at a small volume fraction or an anodic barrier to inhibit the corrosion at a large volume fraction. Chen [10] showed that in 0.1 M sodium sulfate solution, localized corrosion occurred on AZ91 magnesium alloy with the immersion time over 181 h. Jönsson et al. [7] conducted atmospheric corrosion of field exposed magnesium alloy AZ91D in urban, rural and marine environment. They concluded that the boundary between the α -phase and the eutectic α -/ β -phase was sensitive to initiation of corrosion attacks. Yet few investigations were conducted to research the atmospheric corrosion behavior of AZ91D by electrochemical tests.

The aim of present work was to research the effects of TEL thickness and alloy microstructure on the corrosion behavior of AZ91D. Thus, nondestructive electrochemical measurements i.e. EIS, EN and cathodic polarization curves were employed under the TELs in 3.5 wt. % NaCl solutions. Moreover, the characterization techniques of SEM/EDAX and SKPFM were applied to determine the microstructure and distribution of surface potential respectively.

2. EXPERIMENTAL

2.1 Materials and Characterization

Specimens used in the current research were AZ91D magnesium alloy plates cut from an as-cast commercial ingot. The chemical composition (wt. %), given by SPECTROMAXx, was 9.51 Al, 0.95 Zn, 0.175 Mn, 0.034 Si and Mg for balance. The working area was mechanically ground by SiC papers through 400 to 1000 grades, followed by polishing with 1.0 μm Al_2O_3 , rinsed with distilled water, degreased with acetone, and then dried in a cool air flow for standby use.

For metallographic characterization, nital (5 mL HNO₃ + 95mL C₂H₅OH) was used to reveal the microstructure of AZ91D alloy with immersing for 7-10 s. SEM (Hitachi SU8010, Japan) equipped with EDAX was used to observe the metallographic structure and constitution.

Bruker AFM series MultiMode 8 was applied to character the surface topography and the relative Volta potential differences of different micro-constituents of the AZ91D specimens (Φ10 mm, the thickness of 1 mm) using the electrically conducting Au-coated silicon AFM Probes (Multi75GB-G with resonance frequency of 75 kHz and force constant of 7.4 N/m) with the tapping/lift mode sequence at room temperature under a controlled relative humidity of 60-70%.

2.2 The TEL setup

The TEL setup employed in this study is shown in Fig. 1(a). The primary principle of this apparatus is to keep the TEL formed on the working area even and stable, and thickness of TEL was determined by a sharp Pt needle and a micrometer attached on an iron, which are based on our previous research [4].

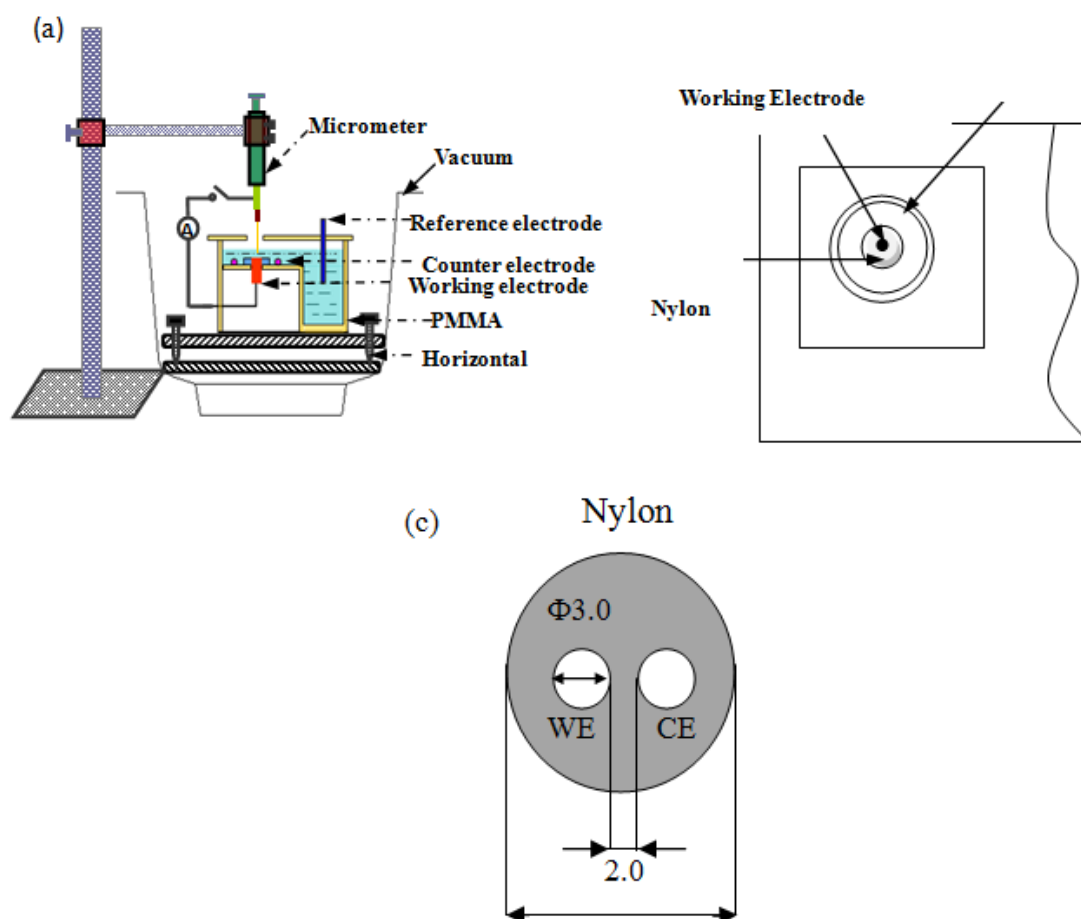


Figure 1. Schematic diagram of the arrangement for TEL study (a) transverse cross-sectional view of the electrochemical cell, (b) directional view of the cell and (c) the top view of electrode for EN measurement.

The diameter of working electrode was 4 mm for EIS and cathodic polarization curve tests and 3 mm for EN test. The side surface of the electrode was sealed by nylon which is more hydrophilic than other materials such as Teflon to ensure only the top surface exposed in the corrosive solution. The working electrode sealed by nylon was fixed tightly in the center of the electrochemical cell consisting of polymethyl methacrylate (PMMA). The electrochemical cell was covered with a PMMA lid to avoid evaporation of the electrolyte during experiments, and then the cell was put in the vacuum drier with a gradienter to adjust the horizontal lever.

2.3 Electrochemical measurements

The EIS at open circuit potential (OCP) and cathodic polarization curves under different TELs were obtained by VMP2 multichannel potentiostat (PARC, USA) and CHI630 electrochemical workstation (Chenhua, China) respectively. The employed amplitude of AC voltage was 5 mV followed by the frequency ranging from 100 kHz to 10 mHz for electrochemical impedance measurements. As reported in the literatures [4, 11], owing to the non-uniform of current distribution during anode polarization, so just cathodic polarization curve was measured in current research with the potential sweep rate of 0.5 mV/s and potentials varying from the OCP to -0.4 V. Pt wire with large area was used as counter electrode for electrochemical measurement.

EN usually refers to random fluctuations of the electrical quantities (electrode potential and cell current) in electrochemical systems [12] and can be recorded in situ through special facility. In our present study, EN measurements under different TELs were in situ recorded in the Faraday cage by using a low noise potentiostat/galvanostat Gamry PCI/4-G300 (Gamry, USA) with ESA410 software. A pair of identical AZ91D alloy electrodes with the diameter of 3 mm, acting as the working and counter electrodes respectively, was embedded in nylon in parallel with 2 mm apart, as displayed in Fig. 1(c). Once the electrodes soaked into the 3.5 wt. % NaCl solutions, the potential and current were acquired simultaneously with continuous sampling of 24 h. The measured potential was between the reference and the two nominal electrode couple and the acquired current was between the two nominal electrodes through zero resistance ammeters (ZRA) circuit. The sampling frequency was 5 Hz. Fast Wavelet Transformation (FWT) which transformed the time domain signal to frequency domain information was performed to interpret the possible corrosion process and type according to the energy distribution plots (EDPs) [13]. The original signal was decomposed to two coefficients, namely, the smoothing coefficient (S_j) and detail coefficient (d_j) through the use of Daubechies wavelets "db4" orthogonal. Both the detail and smoothing coefficients are defined as crystals with the reflecting of local information and the general trend of the original signal, respectively. Noise resistance (R_n), defined as standard deviation of potential divided by standard deviation of current ($R_n = \sigma_E / \sigma_I$), is an effective method to monitor and assess the corrosion rate [14, 15]. Normally R_n is inversely proportional to the corrosion rate of the electrode for many cases.

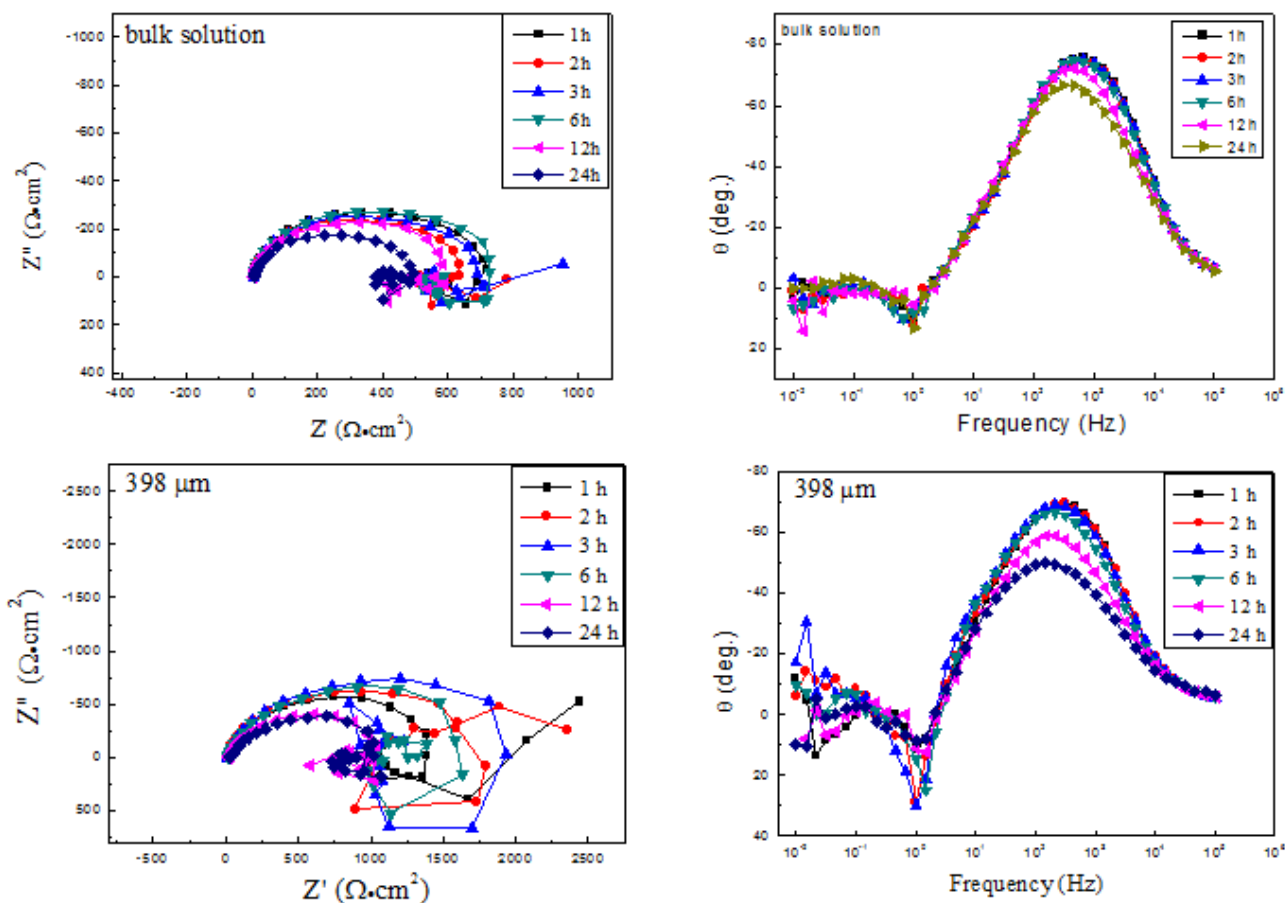
To ensure the thickness of the covered electrolyte constant during the immersion time, the device was carefully sealed by vaseline. All electrochemical measurements used the saturated calomel

electrode (SCE) as reference electrode and neutral 3.5 wt. % NaCl solution as the electrolyte. Deionized water and analytical grade reagent were used.

3. RESULTS AND DISCUSSION

3.1 EIS behavior

EIS, a nondestructive measurement, was conducted to obtain information of corrosion progress under different TELs with the evolution of time, which can reveal the mechanistic of the atmospheric corrosion of various alloys [16, 17]. The EIS results of AZ91D alloy under given TEL thicknesses and in bulk solutions up to the immersion time of 24 h are depicted in Fig. 2. From the Nyquist plots shown in Fig. 2, the EIS of AZ91D alloy display different shape with the variation of electrolyte thickness and immersing time. Based on combination of our previous works [6, 18] and EIS plots shown in Fig. 2, three time constants are observed and the time constants at high frequencies (HFs) and intermediate frequencies (MFs) are partly overlapped. In detail, under bulk solution and the layer thickness of 398 and 305 μm , the impedance spectra consist of two capacitive arcs corresponding to HFs and MFs respectively, which are attributed to the performance of the surface film and charge transfer behavior respectively [19].



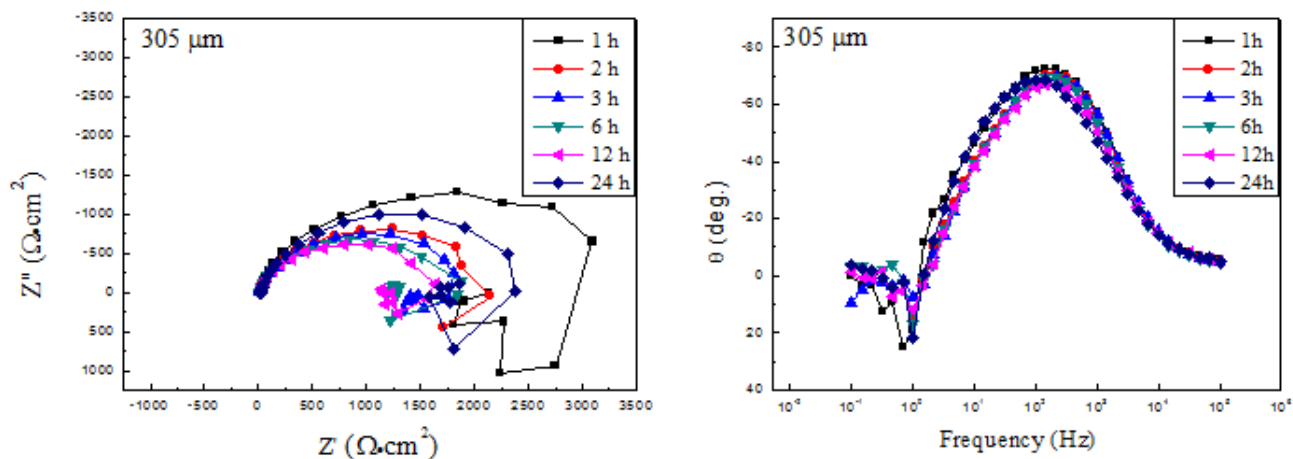
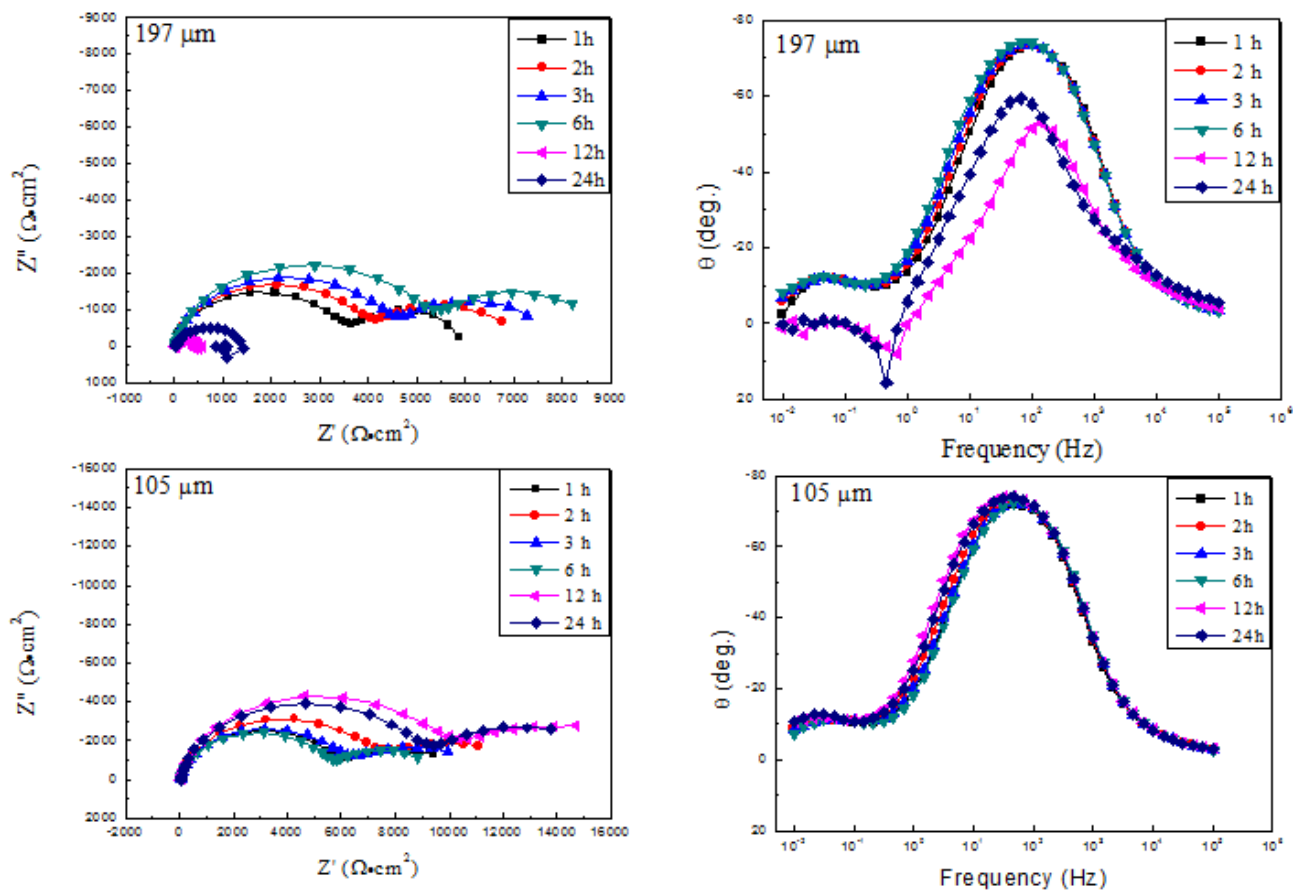


Figure 2. Experimental Nyquist and Bode plots of AZ91D alloy under given TEL thickness from bulk solution to 305 μm during 24 h immersion in 3.5 wt. % NaCl solution.

Moreover, at low frequencies (LFs), another arc reveals an inductive behavior. For the inductive phenomena appeared in LFs, many examples have been found and various explanations have been proposed, mainly including the relaxation of adsorbed species in the corrosion process [20, 21] and the formation of localized corrosion [22, 23]. In the present research, it is considered that the inductive arcs may be related to the gathering of surface electrically active species on the bare substrate, for instance, adsorbed univalent Mg ion (Mg_{ads}^+) [20, 24].



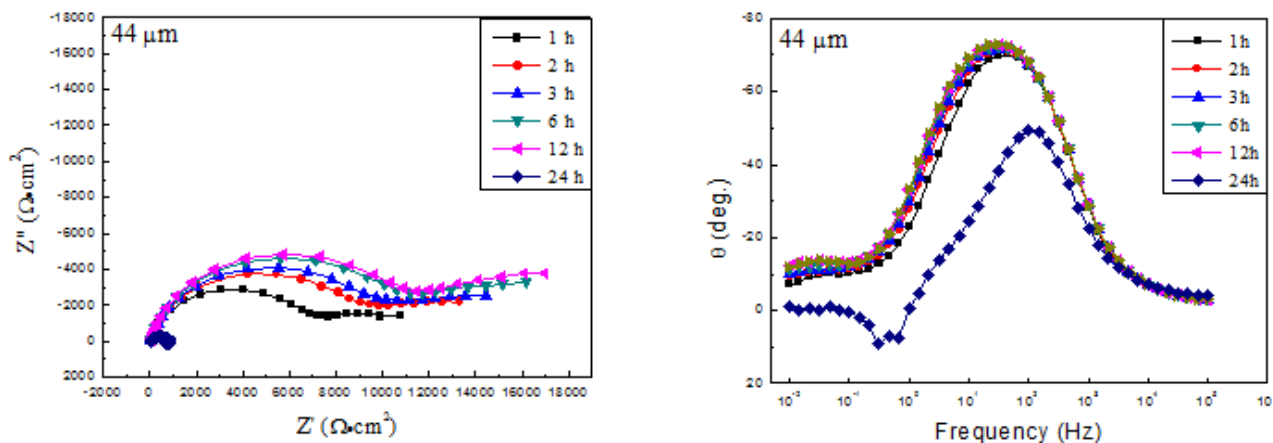


Figure 3. Experimental Nyquist and Bode plots of AZ91D alloy under given TEL thickness from 197 to 44 μm during 24 h immersion in 3.5 wt. % NaCl solution.

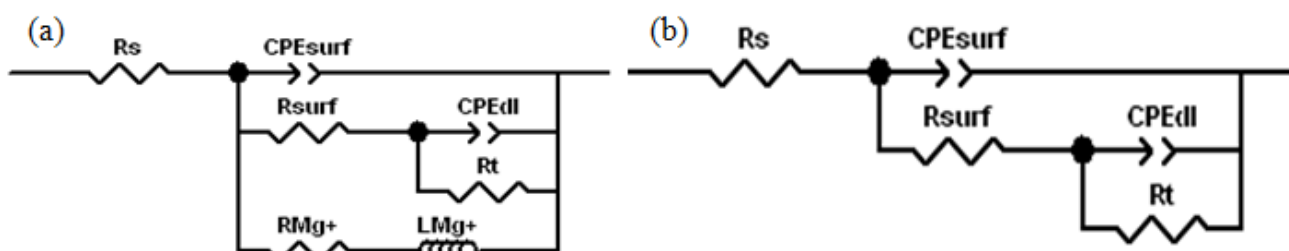


Figure 4. Equivalent circuit models for EIS under TEL in 3.5 wt. % NaCl solution: (a) with and (b) without the inductive tails at LFs.

Table 1. The fitting results obtained from equivalent circuit for AZ91D in 3.5 wt. % NaCl under bulk solution, 305 and 44 μm TEL.

TEL Thickness (μm)	Time (h)	R_s ($\Omega \cdot \text{cm}^2$)	$CPE_{surf} \cdot T$ ($\mu\text{F} \cdot \text{cm}^{-2}$)	n_1	R_{surf} ($\Omega \cdot \text{cm}^2$)	$CPE_{dl} \cdot T$ ($\mu\text{F} \cdot \text{cm}^{-2}$)	n_2	R_t ($\Omega \cdot \text{cm}^2$)	$R_{surf} + R_t$ ($\Omega \cdot \text{cm}^2$)
Bulk solution	1	4.28	8.28	0.95	540.35	54.91	1	170.27	710.63
	2	4.36	8.75	0.95	483.68	56.34	1	149.92	633.60
	3	4.41	8.99	0.94	527.03	65.73	1	154.94	681.98
	6	4.51	9.95	0.94	563.35	58.57	1	169.39	732.75
	12	4.75	15.04	0.91	495.24	81.17	1	91.46	586.70
	24	5.06	24.51	0.86	450.88	276.13	1	39.94	490.82
305 μm	1	16.27	81.12	0.90	2373.34	223.61	1	870.78	3244.12
	2	15.59	102.65	0.88	1780.00	1.058	1	238.14	2018.14
	3	15.75	90.72	0.89	1444.4	156.78	1	423.52	1867.92
	6	15.67	99.47	0.90	1333.75	230.77	1	405.06	1738.81
	12	16.03	144.83	0.85	1368.41	5.24	1	247.06	1615.47
	24	17.06	120.96	0.86	94.26	11.70	1	2355	2449.26
44 μm	1	57.03	11.94	0.88	6951.97	812.41	0.72	4626.06	11578.03
	2	56.10	12.02	0.88	8986.21	651.74	0.66	7054.13	16040.34
	3	55.08	12.25	0.88	9719.21	600.01	0.65	8173.93	17893.13
	6	53.03	12.41	0.88	10984.52	598.42	0.69	9763.32	20747.83
	12	53.28	12.33	0.89	11464.17	635.03	0.75	10142.44	21606.62
	24	50.87	25.54	0.89	717.41	307.17	1	87.29	804.70

In addition, Fig. 3 discloses the EIS results of AZ91D alloy under thinner given TEL thicknesses up to the immersion time of 24 h. Compared to the EIS shown in Fig. 2, changes on the size of the capacitive loops and the existence of inductive arcs can be observed. Evidently, for the TEL thicknesses of 197, 105 and 44 μm , the EIS consist of two capacitive arcs only with inductive arcs at LFs disappearing for most measuring time. Moreover, as shown in Fig. 3 for almost all immersion time, the diameters at HF and MF of the thicknesses for 197, 105 and 44 μm are much larger than that of the thicker electrolyte layers. Therefore, the corrosion resistance of AZ91D Mg alloy under thinner TELs is higher than that of the thicker ones [25].

From the Bode plots in Fig. 2 and 3, the majority of the phase angle exceeds -45° , meaning that the current distribution is uniform on the electrode surface [16]. Therefore, the obtained results are considered reliable to describe the corrosion behavior of AZ91D under TELs.

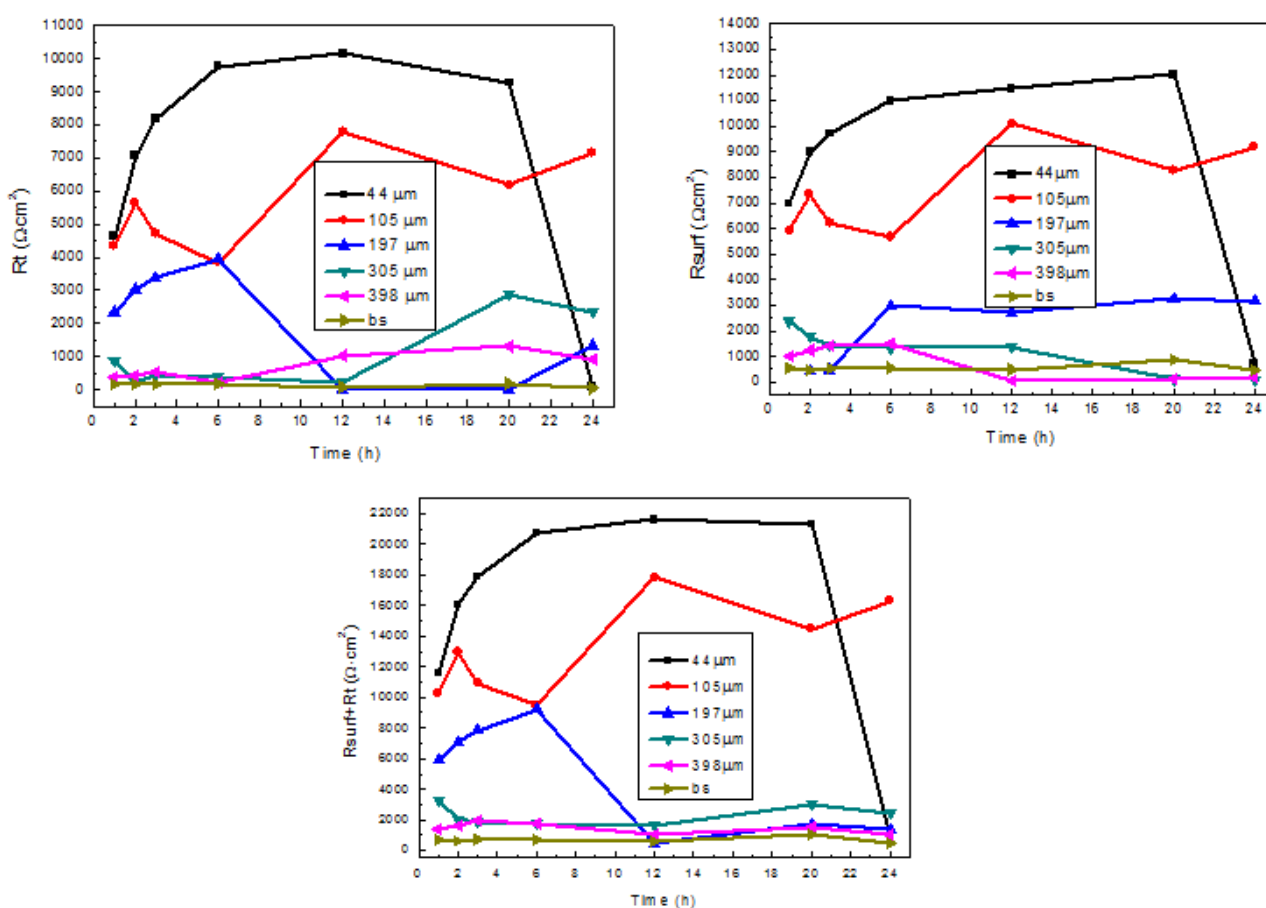


Figure 5. Variation of R_{surf} , R_t and $(R_{surf}+R_t)$ for AZ91D under TEL with different thickness and bulk solution (bs in Figure).

In order to quantitatively investigate the influence of TEL thickness on the atmospheric corrosion behavior of AZ91D magnesium alloy in NaCl solution, combining EIS data with the reference [6, 26, 27], the equivalent circuit models in Fig. 4 are employed to illustrate the corrosion process, where R_s is solution resistance between the reference and working electrodes and its value reflects the electrical conductivity of electrolytes, R_{surf} is on behalf of the resistance of surface film, R_t is charge resistance, CPE_{surf} and CPE_{dl} represent constant phase elements of the surface film and

electric double layer, which are in parallel with R_{surf} and R_t respectively. For the inductive section, R_{Mg^+} relates to reaction resistance of Mg_{ads}^+ that acts as the adsorbed intermediates formed on the alloy AZ91D surface, while L_{Mg^+} is relevant to inductive resistance of Mg_{ads}^+ reaction. Some typical parameters except the fitting results of the inductive loops obtained from equivalent circuit for AZ91D under different TELs are presented in Table 1.

As shown in Table 1, the values of R_s under TELs are larger than that of bulk solution during the immersion time and increase with the TEL thickness decreasing, indicating the TELs can increase the ohmic drop and benefiting from the device used the values of ohmic drop under TELs are acceptable. The values of R_t , R_{surf} , and $(R_{surf}+R_t)$ of the fitting results are important information related to the corrosion process. As mentioned above and Song's work [19], R_{surf} can be also used as one of the parameters for corrosion characterization, therefore the value of $(R_{surf}+R_t)$ is usually employed to describe the corrosion resistance. From the three sets of data in Table 1, $(R_{surf}+R_t)$ values increase with the thinning of the electrolyte layers, showing the enhancement of the corrosion resistance. The detail data of R_t , R_{surf} , $(R_{surf}+R_t)$ as functions of the exposure time from bulk solution thinning to the TEL thickness of 44 μm are displayed in Fig. 5. In general, the sum of R_t and R_{surf} shows the lowest number in bulk solution and increases with the TEL thinning. It is also clear from Fig. 5 that R_t shows intimately relate to R_{surf} for the thickness of 105 and 44 μm , that is R_t increases with the increasing of R_{surf} for most exposure time. For the corrosion behavior of magnesium alloy under very thin electrolyte layer (ca. 44 μm), the diffusion of the corrosion products to bulk solution is very difficult, and because of the increase of local pH and more corrosion products are accumulated on the alloy surface, both of which can lower the corrosion rate by inhibiting the anodic process to a large degree [5]. During the exposure time, the variation of $(R_{surf}+R_t)$ is not obvious for TEL thickness over 197 μm , but for thinner thickness in the initial time the value increases following by a decrease and then keeps relatively stable except for the thickness of 44 μm . The values of R_{surf} and R_t decrease dramatically to a very low level at the 24 h immersion for this thin thickness, mainly due to the rupture of the protective film. From the observation above, it is clear that the corrosion resistance of AZ91D is enhanced under TELs compared with bulk solution and increases with the TEL thinning, which mainly results from the formation of more protective surface film produced by the accumulation of corrosion products.

3.2 Electrochemical noise behavior

Fig. 6 shows the typical representative of electrochemical potential and current noise signal under TEL thickness of around 50 μm after immersing for 100 s in 3.5 wt. % NaCl solution. Take the potential transients into account, as shown, the potential keeps stable at first and then shifts abruptly to negative direction, followed by a partly increase, meanwhile the sudden increases arise in current transition, which can be attributed to pit initiation. Moreover, what must be noticed is that a few potential decreases and then up to the background level following, which may be the propagation and repassivation of pits according to many reports [14, 28, 29]. Those changes referred to mean that localized corrosion happened on the AZ91D surface. However, only the original time series signal is

not enough to depict the corrosion evolution during corrosion detection and monitor. In order to understand the information comprehensively, it is necessary to set up some available methods. FWT and average R_n method are employed in the present study.

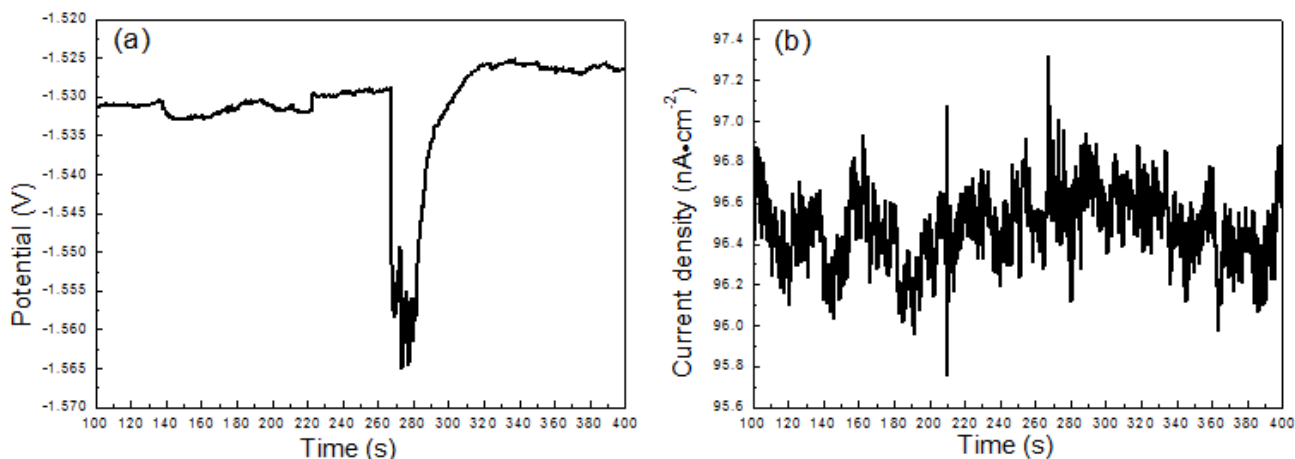


Figure 6. Typical potential (a) and current (b) fluctuations for AZ91D immersion under 50 μm TEL in 3.5 wt. % NaCl solution after 100s.

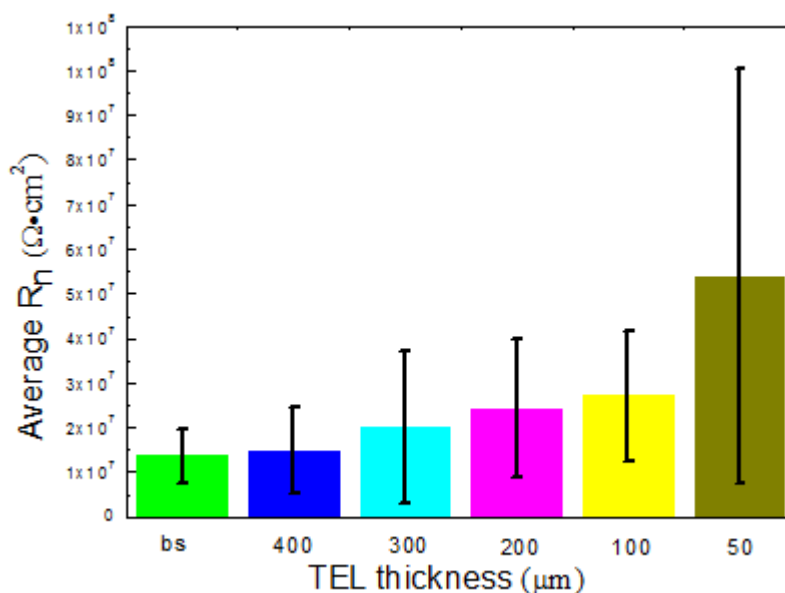


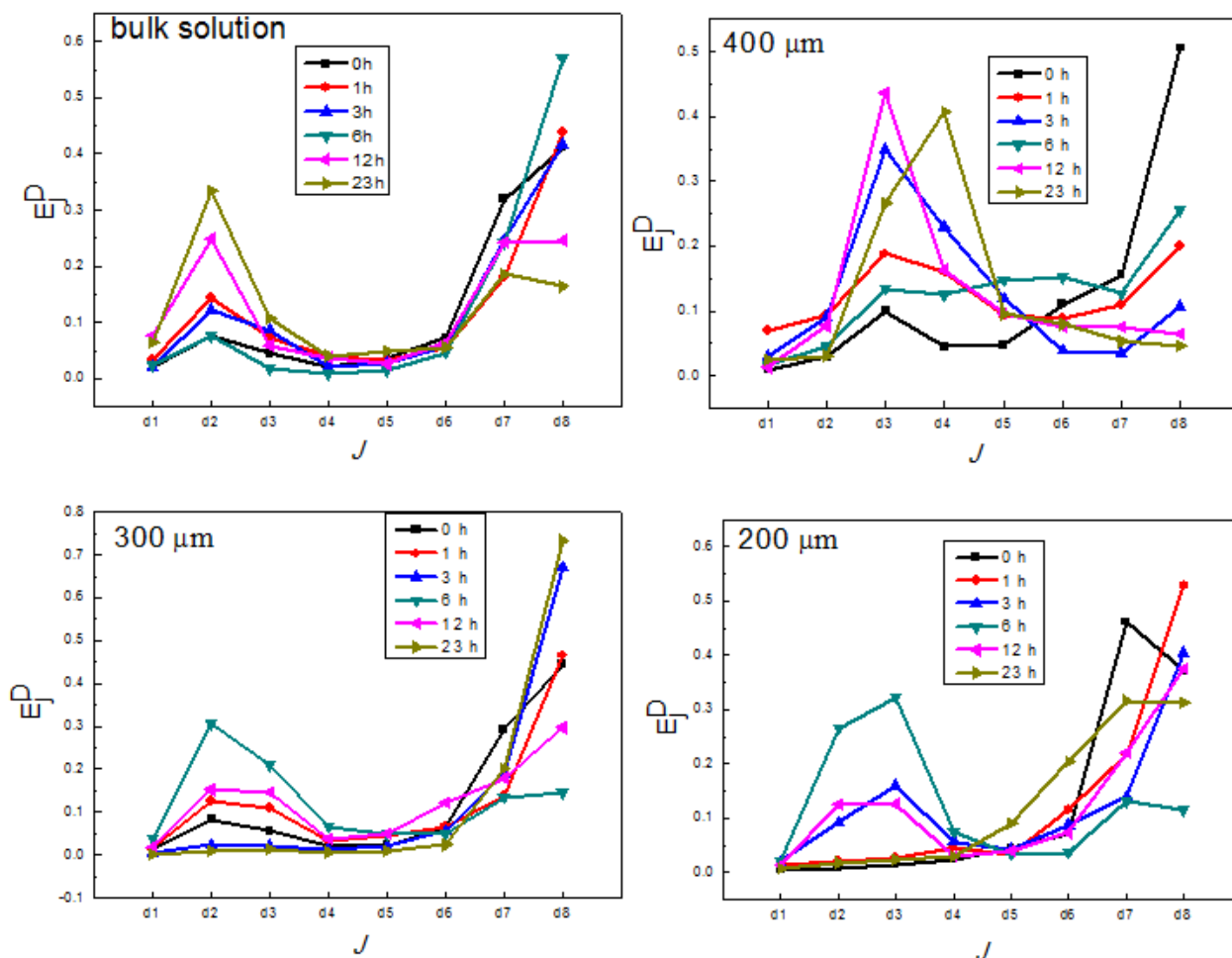
Figure 7. Average noise resistance (R_n) values for the corrosion on AZ91D under given TEL thickness during the exposure time of 24 h.

The electrochemical potential and current noise with the length of 2048 data points after 10 minutes of each hour under different thickness of TEL were extracted to calculate the corresponding R_n . Afterwards average R_n value with the standard deviation for the corrosion on AZ91D during the continuously exposure time of 24 h was counted and demonstrated in Fig. 7 and the error bar values show discrete degree between the individuals. On the basis of the Fig. 7, from the bulk solution to

different thickness of TELs, the average R_n rises with the TEL thickness thinning, which is consistent with the $(R_{surf}+R_{ct})$ values from EIS results.

Aballe et al. [28] reported that the fine scale coefficients, d_1-d_3 , corresponding to events of the small time scales, represent the fast process with rapid fluctuations of the original signal in research system. Besides, the energy coefficients d_4-d_8 is related to the original signal of large scale features. Some investigators [13, 29] have confirmed this theory combining the FWT handling method with other morphology characterizations.

FWT was employed to decompose each set of data of electrochemical potential noise with length of 2048 points after 10 minutes of each hour under different thickness of TEL. The energy coefficients (d_1-d_8) of each set of wavelet are plotted in Fig. 8. The energy of the wavelet coefficients of d_1-d_3 is much smaller compared to d_7-d_8 after immersion 10 minutes under all TELs and bulk solution, which mainly due to the uniform corrosion of the surface film formed in air [13]. In the case of electrode in bulk solution, the energy of d_1-d_3 increases except the expose of 6 h, indicating that the possibility of fast process may increase with time increasing. However, it is also obvious that the energy of d_7-d_8 is predominant for the whole exposure time. Hence, dominated relative energy in the region of d_7-d_8 illuminates that the electrode shows a behavior of uniform corrosion.



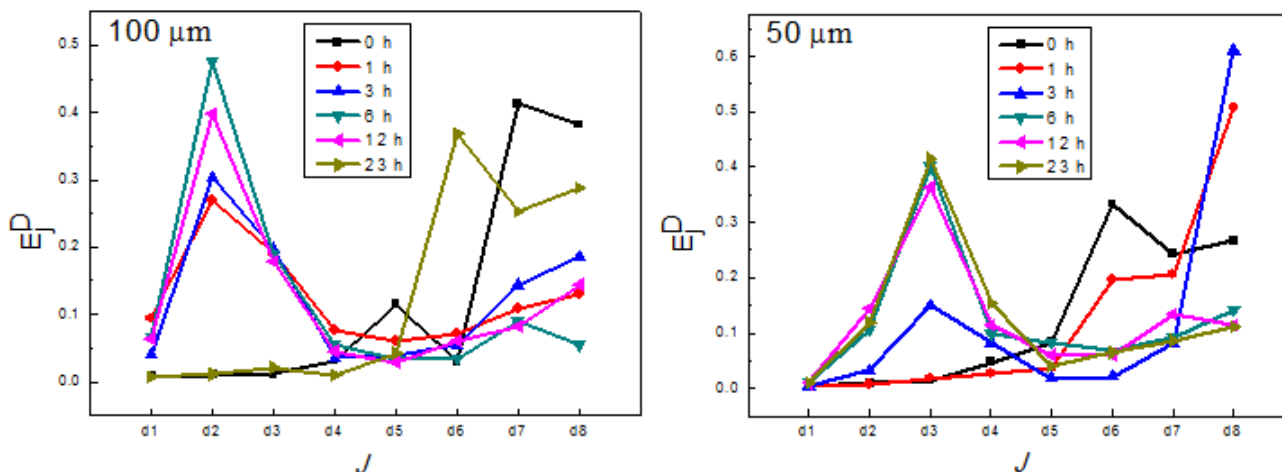


Figure 8. Energy distribution plots (EDPs) of the detail coefficient set, d_1, d_2, \dots, d_J (the energy is normalized) corresponding to the potential noise signal.

For the TEL thickness of around 400 μm , the EDPs trend seems similar with the bulk solution with time increasing, however, the value of the absolute energy of crystals present much different with J changing. In especial, the energy in d_3 at the time of 3, 12 h and d_4 for 23 h is outstanding, meaning that fast events are dominated, which can be seen at the SEM image in Fig. 10 that shows localized corrosion around the β phase occurs. For the TEL thicknesses of around 300 and 200 μm , the energy distribution trend roughly has the same shape, while the fast events of the electrode have the highest energy at the immersion time of 6 h. For the thickness of around 100 and 50 μm in most immersion time (except 0 and 23 h for 100 μm and 0-3 h for 50 μm), the relative energy concentrates in the region of d_1 - d_3 with the outstanding value in d_2 and d_3 respectively. Above all, the corrosion behavior of AZ91D under TEL and bulk solution shows difference during the exposure time. Uniform corrosion is the main type for bulk solution, while localized corrosion turns up and increases with the TEL thickness thinning for electrodes, which can be verified with the SEM images below. For 100 and 50 μm TEL, localized corrosion is the main corrosion type.

3.3 Cathodic polarization behavior

The cathodic polarization curves for AZ91D from bulk solution to 50 μm at immersion time of 1 h in 3.5 wt. % NaCl are presented in Fig. 9. The evident Tafel region is shown and it's clear that the cathodic current densities under TEL are lower than that in bulk solution, indicating the cathodic progress is inhibited under TEL.

Using the Tafel extrapolation method, the corrosion potential (E_{corr}), corrosion current density (I_{corr}) at the free corrosion potential and the cathodic Tafel slop (β_c) values are calculated, which are displayed in Table 2. From the Evans diagram of corrosion system, the increase of corrosion potential comes from two parts, i.e. the inhibition of the anodic progress or the acceleration of the cathodic process. In present research the corrosion potentials shift to higher values with TEL thickness decreasing, meanwhile the depressed cathodic progress is observed from Fig. 9, elucidating the anodic

progress might be inhibited under TEL. The I_{corr} values decrease evidently with the decreasing of TEL thickness especially from the thickness of 300 to 200 μm . The variation of β_c can be neglected during the TEL thickness varying, implying the cathodic behavior in different TEL is similar.

As generally believed [30, 31], the cathodic reaction of Mg alloy in NaCl solution is hydrogen evolution.

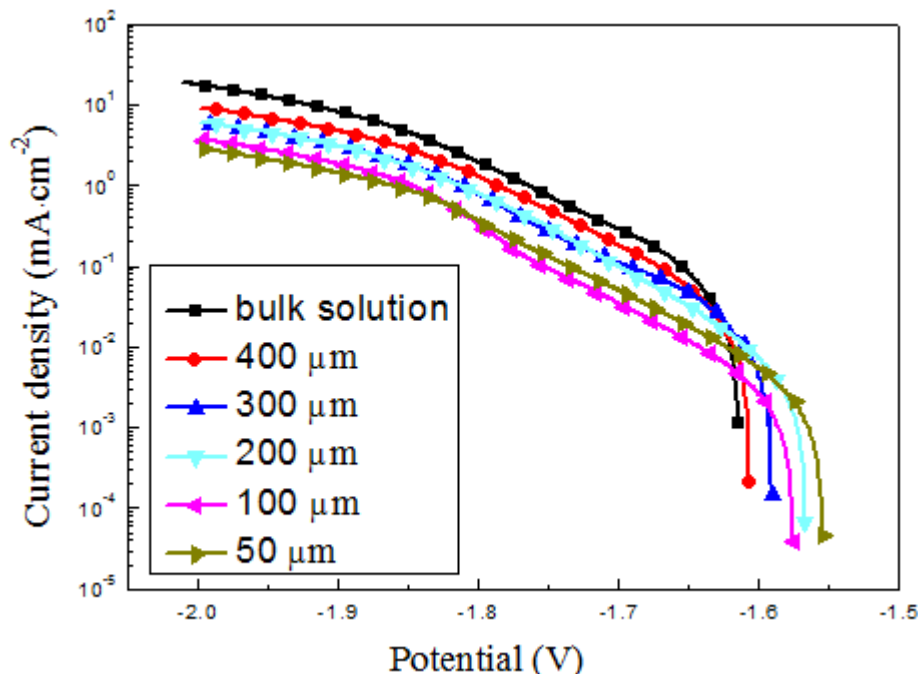


Figure 9. Cathodic polarization curves for AZ91D under various TEL thicknesses at exposure time of 1 h in 3.5 wt. % NaCl.

Hydrogen evolution occurs according to above equation, which is in accordance with the phenomenon of bubbles generating on the electrolyte surface observed during the process of cathodic polarization. In bulk solution and thick TEL thickness the generated OH^- can diffuse in time, however the diffusion is greatly inhibited with the TEL thinning to some extent. So the concentration of OH^- at the cathodic regions increase, resulting in the local alkalization.

Table 2. The results obtained from cathodic polarization curves for AZ91D under various TEL thicknesses at exposure time of 1 h in 3.5 wt. % NaCl.

Thickness (μm)	Bulk solution	~ 400	~ 300	~ 200	~ 100	~ 50
E_{corr} (V vs SCE)	-1.614	-1.607	-1.591	-1.567	-1.576	-1.555
I_{corr} ($\text{mA}\cdot\text{cm}^{-2}$)	0.0525	0.0283	0.0164	0.00498	0.00273	0.00266
β_c ($\text{mV}\cdot\text{dec}^{-1}$)	119.48	115.49	131.10	102.61	113.31	114.14

As the decrease of the TEL, it's beneficial to the formation of main corrosion products $Mg(OH)_2$ resulting from the increase of local pH, protecting AZ91D alloy from further corrosion by restricting the reaction of Mg. According to the above analysis, the anodic and cathodic processes are both depressed under TEL in the corrosion of AZ91D alloy in 3.5 wt. % NaCl.

3.4 Characterization

After exposure in 3.5 wt. % NaCl solution with different TEL thickness and bulk solution, SEM/EDAX was used to characterize the electrode surface morphology and composition. Fig. 10 illustrates the SEM images for AZ91D under various TEL thicknesses after exposure of 1 h; the insert figures presented at the upper right corner of the basic images are the enlarged view of the interesting character. Fig. 10 reveals that corrosion pits along with corrosion products appear for bulk solution and all TEL thicknesses, indicating that at the initial corrosion stage the form of localized corrosion is primary. It is also visible that the corrosion degree in bulk solution is much severer than that under TELs and diminishes with TEL thickness decreasing. From the EDAX results (Atomic %) of the corrosion products forming on AZ91D surface under some representative TEL thicknesses after 1 h immersion in 3.5 wt. % NaCl solutions shown in Table 3, the main composition elements of the corrosion products are Mg, O and a small amount of Al and the oxygen content reduces with the thinning of the TELs.

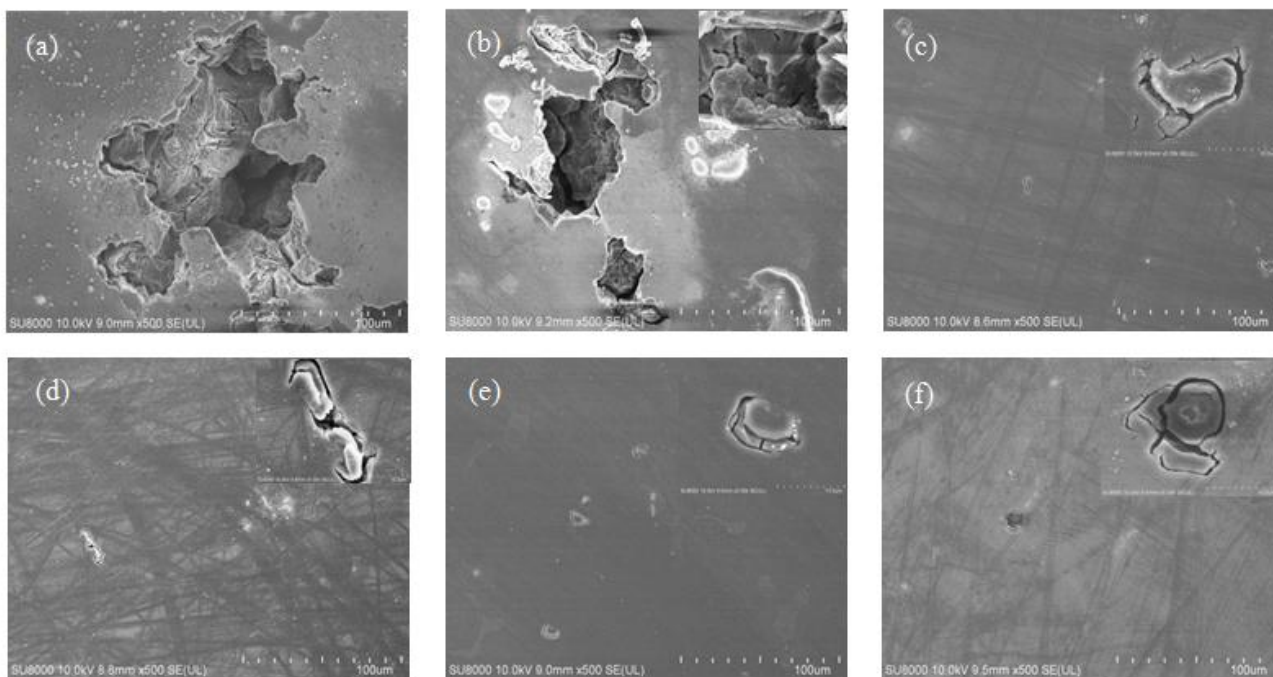


Figure 10. SEM images for AZ91D under various TEL thicknesses at exposure time of 1 h in 3.5wt. % NaCl (a) in the bulk solution and under (b) 400 μm , (c) 300 μm , (d) 200 μm , (e) 106 μm and (f) 57 μm .

Both the SEM and the corresponding EDAX results after exposure for 1 h reveal the alike changing trend of the corrosion rate, namely, the corrosion rate decreases with the TEL thickness thinning at the initial stage, which is in agreement with the result obtained from EIS and average R_n result. Moreover, localized corrosion pits formed around the noble particles show up under the TELs verified the FWT results of EN experiments.

Table 3. The EDS results (at. %) of the corrosion products of AZ91D under some representative TEL thicknesses after 1 h immersion in 3.5 wt. % NaCl solutions.

Thickness	Mg	O	Al	Mg/O
bulk solution	51.246	43.237	5.518	1.185
400 μm	52.56	38.41	9.03	1.368
106 μm	66.359	29.175	4.467	2.275

As exposure time prolongs to 24 h, the changes on the electrode morphology are displayed in Fig. 11. Compared with the exposure time of 1 h, a significant difference on the visual appearance of electrode surface is that the surface is severely damaged with the corrosion pits and covered with corrosion products. Additionally, the exposure in bulk solution shows heaviest uniform corrosion attack than others, which is consistent with the corrosion rate obtained from electrochemical measurements discussed above.

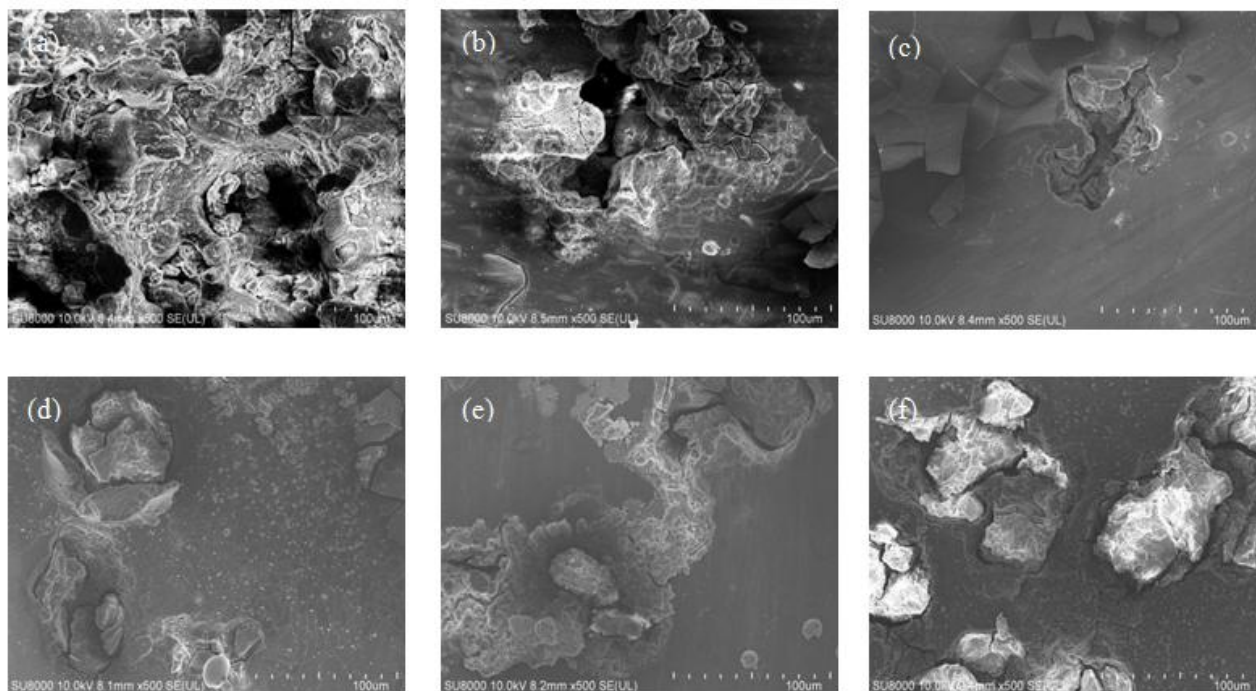


Figure 11. SEM images for AZ91D under various TEL thicknesses at exposure time of 24 h in 3.5wt. % NaCl (a) in the bulk solution and under (b) 396 μm , (c) 300 μm , (d) 197 μm , (e) 100 μm and (f) 58 μm .

For the corrosion under TELs, the AZ91D substrate around the noble β phase suffers extensive corrosion, even for some TELs the noble particles fall off and crevice corrosion occurs. Therefore, pitting corrosion and subsequent crevice corrosion are the main corrosion type of AZ91D under TELs, which further proves the EN results.

It is well known metal corrosion usually results from the micro-galvanic couples. For the pitting corrosion occurred, the following study of distribution of the surface Volta potential by SKPFM may give an interpretation. Fig. 12 (a) shows the microstructure of the etching surface of AZ91D. According to the EDAX results the measured at. % concentrations of the β phase is 2.335 % for O, 62.299 % for Mg, 33.657% for Al and 1.709% for Zn, showing an Mg/Al atomic ratio of 1.85 which is close to the stoichiometric ratio of $Mg_{17}Al_{12}$.

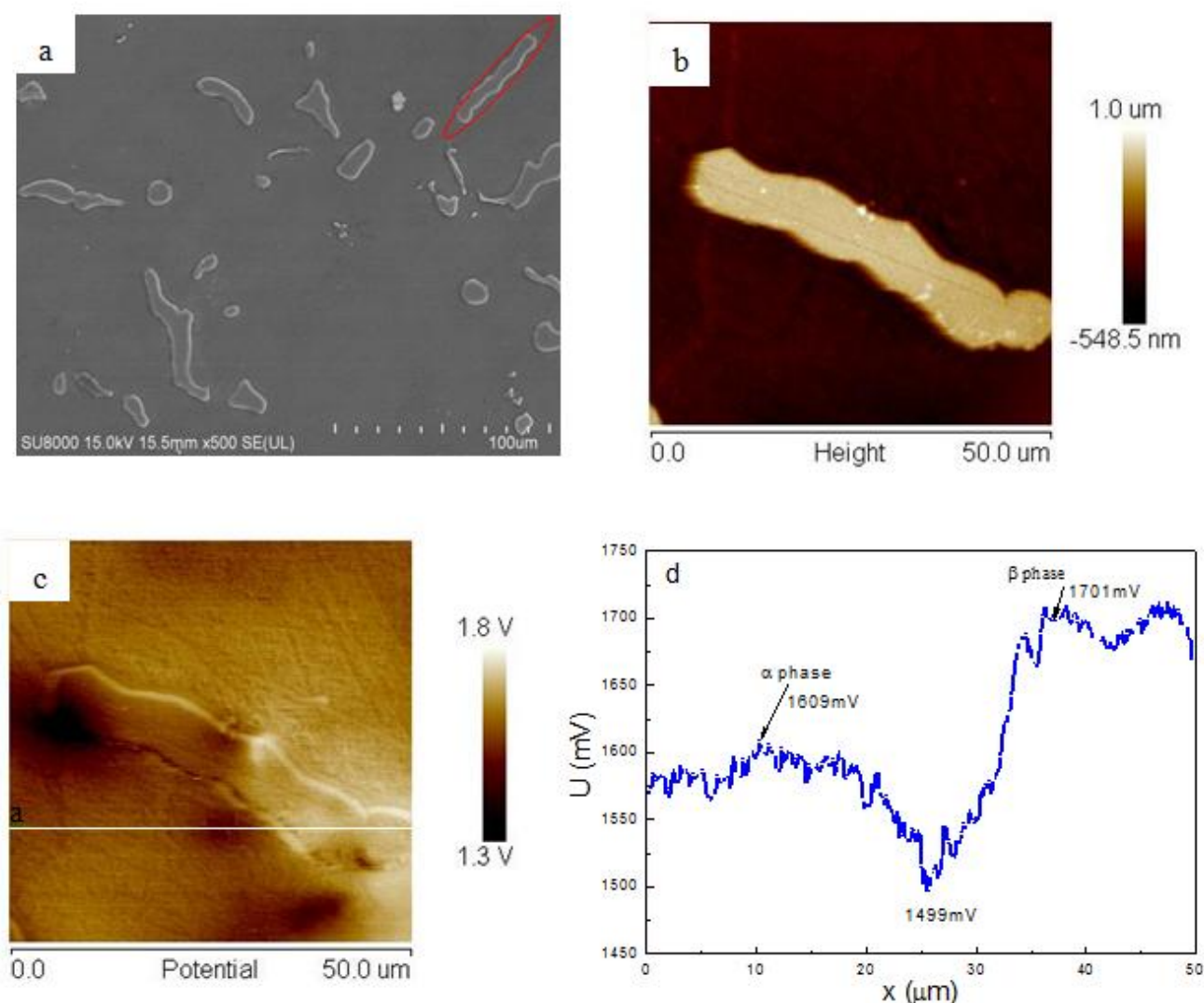


Figure 12. (a) Microstructure, (b) topography surface, (c) potential map and (d) potential profile analysis for AZ91D alloy after etching.

Moreover, SKPFM was utilized to measure the Volta potential difference between the substrate α phase and β phase marked with a red circle in microstructure image. Liu [6] has stated that the alloy

composition has an impact on Volta potential difference between α and β phases for AM50 magnesium alloy. In the current research, as shown in Fig. 12, the β phase shows a clear distinction to the substrate α phase in both topography and potential maps. The Volta potential profile indicates that the potential difference between β phase and α phase is 92 mV, meanwhile the difference between β phase and the adjacent matrix is up to 202 mV. Thus β phase is liable to act as cathodic zone with respect to the matrix and the adjacent matrix clearly manifests the most susceptible to corrosion, which was verified by other workers [32].

4. CONCLUSION

The corrosion behavior of AZ91D magnesium alloy under various TEL thicknesses in 3.5 wt. % NaCl solution was investigated through nondestructive EIS, EN and cathodic polarization methods, from which it is appreciated that the corrosion behavior under TELs shows great difference with that in bulk solution. The corrosion resistance is enhanced under TELs compared to bulk solution and the corrosion rate decreasing with the TEL thinning. The cathodic reaction of AZ91D is hydrogen evolution, and both anodic and cathodic reactions are restrained under TELs, especially in thickness thinning to around 200 μm and lower. The FWT analysis of the EN data and the morphology obtained from SEM further manifest that the uniform corrosion is the main corrosion type in bulk solution, whereas pitting corrosion around the noble β phase particles and crevice corrosion are dominant under TELs.

ACKNOWLEDGEMENT

This work was supported by National Natural Science Foundation of China (Nos. 51131005 and 51171172), Zhejiang Provincial Natural Science Foundation of China (No. LR16E010001), Fundamental Research Funds for the Central Universities (No. 2015QNA3011) and Science and Technology Commission of Shanghai Municipality (No: 14DZ2261000).

Reference

1. H. Katayama, K. Yagi, A. Nshikata and T. Tsuru, *Electrochim. Acta*, 41 (1996) 1093.
2. Y. Chen, D.M. Qi, H.P. Wang, Z. Xu, C.X. Yi and Z. Zhang, *Int. J. Electrochem. Sci.*, 10 (2015) 9056.
3. A. Nishikata, Y. Ichihara and T. Tsuru, *Corros. Sci.*, 37 (1995) 897.
4. Y.L. Cheng, Z. Zhang, F.H. Cao, J.F. Li, J.Q. Zhang, J.M. Wang and C.N. Cao, *Corros. Sci.*, 46 (2004) 1649.
5. T. Zhang, C.M. Chen, Y.W. Shao, G.Z. Meng, F.H. Wang, X.G. Li and C.F. Dong, *Electrochim. Acta*, 53 (2008) 7921.
6. W.J. Liu, F.H. Cao, A.N. Chen, L.Y. Zheng, J.Q. Zhang and C.N. Cao, *Corros. Sci.*, 52 (2010) 627.
7. M. Jönsson, D. Persson and C. Leygraf, *Corros. Sci.*, 50 (2008) 1406.
8. M. Esmaily, M. Shahabi-Navid, J.E. Svensson, M. Halvarsson, L. Nyborg, Y. Cao and L.G. Johansson, *Corros. Sci.*, 90 (2015) 420.
9. G.L. Song, A. Atrens, X.L. Wu and B. Zhang, *Corros. Sci.*, 40 (1998) 1769.
10. J. Chen, J.Q. Wang, E.H. Han, J.H. Dong and W. Ke, *Electrochim. Acta*, 52 (2007) 3299.
11. M. Stratmann, H. Streckel, K.T. Kim and S. Crockett, *Corros. Sci.*, 30 (1990) 715.

12. U. Bertocci and F. Huet, *Corrosion*, 51 (1995) 131.
13. F.H. Cao, Z. Zhang, J.X. Su, Y.Y. Shi and J.Q. Zhang, *Electrochim. Acta*, 51 (2006) 1359.
14. M. Behzadnasab, S.M. Mirabedini, K. Kabiri and S. Jamali, *Corros. Sci.*, 53 (2011) 89.
15. G. Montesperelli and G. Gusmano, *Corros. Rev.*, 29 (2011) 247.
16. A. Nishikata, Y. Ichihara and T. Tsuru, *Corros. Sci.*, 53 (1997) 897.
17. H.L. Huang, Z.H. Dong, Z.Y. Chen and X.P. Guo, *Corros. Sci.*, 53 (2011) 1230.
18. W.J. Liu, F.H. Cao, B.G. Jia, L.Y. Zheng, J.Q. Zhang, C.N. Cao and X.G. Li, *Corros. Sci.*, 52 (2010) 639.
19. G.L. Song and Z.M. Shi, *Corros. Sci.*, 85 (2014) 126.
20. G. Galicia, N. Pébère, B. Tribollet and V. Vivier, *Corros. Sci.*, 51 (2009) 1789.
21. W.J. Liu, F.H. Cao, A.N. Chen, L.R. Chang, J.Q. Zhang and C.N. Cao, *Corrosion*, 68 (2012) 045001.
22. Y.J. Zhang, C.W. Yan, F.H. Wang and W.F. Li, *Corros. Sci.*, 47 (2005) 2816.
23. C.M.A. Brett, L. Dias, B. Trindade, R. Fischer and S. Mies, *Electrochim. Acta*, 51 (2006) 1752.
24. T. Zhang, Y. Li and F.H. Wang, *Corros. Sci.*, 48 (2006) 1249.
25. X.J. Cui, X.Z. Lin, C.H. Liu, R.S. Yang, X.W. Zheng and M. Gong, *Corros. Sci.*, 90 (2015) 402.
26. W. Liu, F. Cao, L. Zhong, L. Zheng, B. Jia, Z. Zhang and J. Zhang, *Mater. Corros.*, 60 (2009) 795.
27. M. Bethencourt, F.J. Botana, M.J. Cano, M. Marcos, J.M. Sánchez-Amaya and L. González-Rovira, *Corros. Sci.*, 50 (2008) 1376.
28. A. Aballe, M. Bethencourt, F.J. Botana and M. Marcos, *Electrochem. Commun.*, 1 (1999) 266.
29. Y. Li, R. Hu, J. Wang, Y. Huang and C.J. Lin, *Electrochim. Acta*, 54 (2009) 7134.
30. R. Lindström, J.E. Svensson and L.G. Johansson, *J. Electrochem. Soc.*, 149 (2002) B103.
31. G. Song, A. Atrens, D. Stjohn, J. Nairn and Y. Li, *Corros. Sci.*, 39 (1997) 855.
32. A. Davoodi, J. Pan, C. Leygraf and S. Norgren, *Electrochem. Solid-State Lett.*, 8 (2005) B21.

© 2016 The Authors. Published by ESG (www.electrochemsci.org). This article is an open access article distributed under the terms and conditions of the Creative Commons Attribution license (<http://creativecommons.org/licenses/by/4.0/>).